J. J. Trans. Phenomena, Vol. 1, pp. 173–190
Reprints available directly from the publisher
Photocopying permitted by license only

© 1999 OPA (Overseas Publishers Association) N.V.
Published by license under
the Gordon and Breach Science
Publishers imprint.
Printed in Malaysia.

An Axisymmetry-Breaking Instability of Axially Symmetric Natural Convection*

ALEXANDER YU. GELFGAT[a,†], PINHAS Z. BAR-YOSEPH[a], ALEXANDER SOLAN[a] and TOMASZ A. KOWALEWSKI[b]

[a]*Computational Mechanics Laboratory, Faculty of Mechanical Engineering, Technion – Israel Institute of Technology, Technion City, Haifa 32000, Israel;* [b]*Center of Mechanics, Polish Academy of Sciences, IPPT, PAN, Swietokrzyska 21, Warsaw 00-049, Poland*

(Received 25 September 1998; In final form 25 January 1999)

The three-dimensional instability of an axisymmetric natural convection flow is investigated numerically using a global spectral Galerkin method. The linear stability problem separates for different azimuthal modes. This allows us to reduce the problem to a sequence of 2D-like problems. The formulation of the numerical approach and several test calculations are reported. The numerical results are successfully compared with an experiment on natural convection of water in a vertical cylinder, which shows an axisymmetry-breaking instability with a high azimuthal wavenumber.

Keywords: Axisymmetry-breaking instability, natural convection, global Galerkin method

INTRODUCTION

Natural convection flows in axisymmetric regions are common in many technological processes and are widely used as experimental and numerical models. When the characteristic temperature difference increases the laminar axisymmetric flow loses its stability and becomes three-dimensional. Such axisymmetry-breaking bifurcations always take place as a stage in the course of laminar-turbulent transition. This study is devoted to the numerical analysis of a particular case when a steady axisymmetric flow becomes unstable with respect to three-dimensional perturbations.

The most common way to study the axisymmetry-breaking instability numerically is by the solution of the full three-dimensional unsteady problem where the axisymmetric solution is taken as an initial state (Neumann, 1990; Wanschura *et al.*, 1996; Verzicco and Camussi, 1997). A stability

*This paper is an extended version based on partial results presented at the 10th International Symposium on Transport Phenomena in Thermal Science and Engineering, Kyoto, 1997, and at the 27th Israel Conference on Mechanical Engineering, Haifa, 1998.

†Corresponding author. E-mail: alexg@cmlp.technion.ac.il.

analysis was applied analytically (Jones and Moore, 1979) or numerically (Hardin *et al.*, 1990; Goldstein *et al.*, 1993) only in a particular case with heating from below, when the initial axisymmetric state is a motionless fluid. However, the 2π-periodicity of axisymmetric flow allows one to reduce the 3D stability problem to a sequence of 2D-like problems. This follows from the possibility to expand the 2π-periodic 3D solution in a trigonometric Fourier series in the azimuthal direction. In view of the orthogonality of the Fourier modes, the *linear* stability problem for each mode separates from other modes. The stability problem for each azimuthal mode does not depend on the azimuthal angle, and therefore it is analogous to the axisymmetric stability problem. Such problems can be studied numerically by the approach which was used by Gelfgat *et al.* (1996) (in the following referred as G) for an axisymmetric case. This approach to the analysis of axisymmetry-breaking bifurcations of convective flows using the global spectral Galerkin method is discussed in the present paper. The formulation of the method and several test calculations are reported. It is illustrated how the three-dimensional stability analysis may be used for the explanation of our recent experimental results (Kowalewski and Cybulski (1997), in the following referred to as KC).

FORMULATION OF THE PROBLEM

Consider a natural convection flow of a Boussinesq fluid in a vertical cylindrical enclosure $0 \le r \le 1$, $0 \le z \le A$. The dimensionless momentum, continuity and energy equations are

$$\frac{\partial u}{\partial t} + u\frac{\partial u}{\partial r} + \frac{v}{r}\frac{\partial u}{\partial \varphi} + w\frac{\partial u}{\partial z} - \frac{v^2}{r} = -\frac{\partial p}{\partial r} + \frac{1}{Re}\left(\frac{\partial^2 u}{\partial r^2} + \frac{1}{r}\frac{\partial u}{\partial r} + \frac{1}{r^2}\frac{\partial^2 u}{\partial \varphi^2} + \frac{\partial^2 u}{\partial z^2} - \frac{u}{r^2} - \frac{2}{r^2}\frac{\partial v}{\partial \varphi}\right), \quad (1)$$

$$\frac{\partial v}{\partial t} + u\frac{\partial v}{\partial r} + \frac{v}{r}\frac{\partial v}{\partial \varphi} + w\frac{\partial v}{\partial z} + \frac{uv}{r} = -\frac{1}{r}\frac{\partial p}{\partial \varphi} + \frac{1}{Re}\left(\frac{\partial^2 v}{\partial r^2} + \frac{1}{r}\frac{\partial v}{\partial r} + \frac{1}{r^2}\frac{\partial^2 v}{\partial \varphi^2} + \frac{\partial^2 v}{\partial z^2} - \frac{v}{r^2} - \frac{2}{r^2}\frac{\partial v}{\partial \varphi}\right), \quad (2)$$

$$\frac{\partial w}{\partial t} + u\frac{\partial w}{\partial r} + \frac{v}{r}\frac{\partial w}{\partial \varphi} + w\frac{\partial w}{\partial z} = -\frac{\partial p}{\partial z} + \frac{1}{Re}\left(\frac{\partial^2 w}{\partial r^2} + \frac{1}{r}\frac{\partial w}{\partial r} + \frac{1}{r^2}\frac{\partial^2 w}{\partial \varphi^2} + \frac{\partial^2 w}{\partial z^2}\right) + Gr\theta, \quad (3)$$

$$\frac{\partial u}{\partial r} + \frac{u}{r} + \frac{1}{r}\frac{\partial v}{\partial \varphi} + \frac{\partial w}{\partial z} = 0, \quad (4)$$

$$\frac{\partial \theta}{\partial t} + u\frac{\partial \theta}{\partial r} + \frac{v}{r}\frac{\partial \theta}{\partial \varphi} + w\frac{\partial \theta}{\partial z} = \frac{1}{Pr}\left(\frac{\partial^2 \theta}{\partial r^2} + \frac{1}{r}\frac{\partial \theta}{\partial r} + \frac{1}{r^2}\frac{\partial^2 \theta}{\partial \varphi^2} + \frac{\partial^2 \theta}{\partial z^2}\right). \quad (5)$$

Here (r, φ, z) are the cylindrical coordinates, $\mathbf{v} = (u, v, w)^T$ is the velocity vector, p is the pressure, θ is the temperature, $Gr = \bar{g}\bar{\beta}\Delta\bar{\theta}\bar{R}^3/\bar{\nu}^2$ and $Pr = \bar{\nu}/\bar{\chi}$ are the Grashof and the Prandtl numbers, $A = \bar{H}/\bar{R}$ is the aspect ratio, $\bar{g}$ is the gravity acceleration, $\bar{\beta}$ is the thermal expansion coefficient, $\Delta\bar{\theta}$ is the characteristic temperature difference, $\bar{\nu}$ is the kinematic viscosity, $\bar{\chi}$ is the thermal diffusivity, and $\bar{H}$ and $\bar{R}$ are the height and the radius of the cavity (the overbar indicates dimensional variables). We assume that the walls of the cylinder are stationary, with the usual boundary conditions, and that there is an arbitrary (but axisymmetric) thermal boundary condition. At this stage we leave this condition slightly general. In the following (see the section Numerical Comparison with Experiment) we shall focus on specific boundary conditions.

Let the basic axially-symmetric steady natural convection flow which corresponds to the boundary conditions be the solution of the system (steady

axisymmetric part of (1)–(5))

$$U\frac{\partial U}{\partial r}+W\frac{\partial U}{\partial z}=-\frac{\partial P}{\partial r}+\frac{1}{Re}\left(\frac{\partial^2 U}{\partial r^2}+\frac{1}{r}\frac{\partial U}{\partial r}+\frac{\partial^2 U}{\partial z^2}-\frac{U}{r^2}\right), \quad (6)$$

$$U\frac{\partial W}{\partial r}+W\frac{\partial W}{\partial z}=-\frac{\partial P}{\partial z}+\frac{1}{Re}\left(\frac{\partial^2 W}{\partial r^2}+\frac{1}{r}\frac{\partial W}{\partial r}+\frac{\partial^2 W}{\partial z^2}\right)+Gr\Theta, \quad (7)$$

$$\frac{\partial U}{\partial r}+\frac{U}{r}+\frac{\partial W}{\partial z}=0, \quad (8)$$

$$U\frac{\partial \Theta}{\partial r}+W\frac{\partial \Theta}{\partial z}=\frac{1}{Pr}\left(\frac{\partial^2 \Theta}{\partial r^2}+\frac{1}{r}\frac{\partial \Theta}{\partial r}+\frac{\partial^2 \Theta}{\partial z^2}\right). \quad (9)$$

The main purpose of this study is to find out when the steady axisymmetric solution $\{U(r,z), W(r,z), P(r,z), \Theta(r,z)\}$ becomes unstable with respect to three-dimensional perturbations.

Consider infinitely small perturbations $\{u, v, w, p, \theta\}$ of the velocity, the pressure and the temperature which depend on the three coordinates (r, φ, z) and time t. The linearized problem for the perturbations can be defined as

$$\frac{\partial u}{\partial t}+U\frac{\partial u}{\partial r}+W\frac{\partial u}{\partial z}+u\frac{\partial U}{\partial r}+w\frac{\partial U}{\partial z}=-\frac{\partial p}{\partial r}+\frac{1}{Re}\left(\frac{\partial^2 u}{\partial r^2}+\frac{1}{r}\frac{\partial u}{\partial r}+\frac{1}{r^2}\frac{\partial^2 u}{\partial \varphi^2}+\frac{\partial^2 u}{\partial z^2}-\frac{u}{r^2}-\frac{2}{r^2}\frac{\partial v}{\partial \varphi}\right), \quad (10)$$

$$\frac{\partial v}{\partial t}+U\frac{\partial v}{\partial r}+W\frac{\partial v}{\partial z}+w\frac{\partial W}{\partial z}-\frac{Uv}{r}=-\frac{\partial p}{\partial \varphi}+\frac{1}{Re}\left(\frac{\partial^2 v}{\partial r^2}+\frac{1}{r}\frac{\partial v}{\partial r}+\frac{1}{r^2}\frac{\partial^2 v}{\partial \varphi^2}+\frac{\partial^2 v}{\partial z^2}-\frac{v}{r^2}+\frac{2}{r^2}\frac{\partial u}{\partial \varphi}\right), \quad (11)$$

$$\frac{\partial w}{\partial t}+U\frac{\partial w}{\partial r}+W\frac{\partial w}{\partial z}+u\frac{\partial W}{\partial r}+w\frac{\partial W}{\partial z}=-\frac{\partial p}{\partial z}+\frac{1}{Re}\left(\frac{\partial^2 w}{\partial r^2}+\frac{1}{r}\frac{\partial w}{\partial r}+\frac{1}{r^2}\frac{\partial^2 w}{\partial \varphi^2}+\frac{\partial^2 w}{\partial z^2}\right)+Gr\theta, \quad (12)$$

$$\frac{\partial u}{\partial r}+\frac{u}{r}+\frac{1}{r}\frac{\partial v}{\partial \varphi}+\frac{\partial w}{\partial z}=0, \quad (13)$$

$$\frac{\partial \theta}{\partial t}+U\frac{\partial \theta}{\partial r}+W\frac{\partial \theta}{\partial z}+u\frac{\partial \Theta}{\partial r}+w\frac{\partial \Theta}{\partial z}=\frac{1}{Pr}\left(\frac{\partial^2 \theta}{\partial r^2}+\frac{1}{r}\frac{\partial \theta}{\partial r}+\frac{1}{r^2}\frac{\partial^2 \theta}{\partial \varphi^2}+\frac{\partial^2 \theta}{\partial z^2}\right) \quad (14)$$

with the boundary conditions

$$a_i\frac{\partial f}{\partial n}+b_i f\Big|_{\Gamma_i}=0, \quad (15)$$

where f represents one of the functions u, v, w or θ. To complete the formulation it is necessary to add conditions of 2π-periodicity of all the functions:

$$f(\varphi+2\pi)=f(\varphi). \quad (16)$$

According to linear stability theory, the time dependence of the perturbation functions $\{u, v, w, p, \theta\}$ may be assumed as $\sim\exp(\lambda t)$, where λ determines the time rate of change of a perturbation. The periodicity conditions (16) allow us to represent the solution of (10)–(15) as Fourier series in the azimuthal direction. Thus, the perturbation functions can be represented as

$$\{u, v, w, p, \theta\}=\exp(\lambda t)\times\sum_{k=-\infty}^{k=\infty}\{u_k(r,z), v_k(r,z), w_k(r,z), p_k(r,z), \theta_k(r,z)\}\times\exp(ik\varphi). \quad (17)$$

Equations for the Fourier coefficients $\{u_k, v_k, w_k, p_k, \theta_k\}$ are obtained after substitution of (17) into

(10)–(16), and neglecting the higher-order terms:

$$\lambda u_k + U\frac{\partial u_k}{\partial r} + W\frac{\partial u_k}{\partial z} + u_k\frac{\partial U}{\partial r} + w_k\frac{\partial U}{\partial z} = -\frac{\partial p_k}{\partial r} + \frac{1}{Re}\left(\frac{\partial^2 u_k}{\partial r^2} + \frac{1}{r}\frac{\partial u_k}{\partial r} - \frac{k^2+1}{r^2}u_k + \frac{\partial^2 u_k}{\partial z^2} - \frac{2ik}{r^2}v_k\right), \tag{18}$$

$$\lambda v_k + U\frac{\partial v_k}{\partial r} + W\frac{\partial v_k}{\partial z} - \frac{Uv_k}{r} = -ikp_k + \frac{1}{Re}\left(\frac{\partial^2 v_k}{\partial r^2} + \frac{1}{r}\frac{\partial v_k}{\partial r} - \frac{k^2+1}{r^2}v_k + \frac{\partial^2 v_k}{\partial z^2} + \frac{2ik}{r^2}u_k\right), \tag{19}$$

$$\lambda w_k + U\frac{\partial w_k}{\partial r} + W\frac{\partial w_k}{\partial z} + u_k\frac{\partial W}{\partial r} + w_k\frac{\partial W}{\partial z} = -\frac{\partial p_k}{\partial z} + \frac{1}{Re}\left(\frac{\partial^2 w_k}{\partial r^2} + \frac{1}{r}\frac{\partial w_k}{\partial r} - \frac{k^2}{r^2}w_k + \frac{\partial^2 w_k}{\partial z^2}\right) + Gr\theta_k, \tag{20}$$

$$\frac{\partial u_k}{\partial r} + \frac{u_k}{r} + \frac{ik}{r}v_k + \frac{\partial w_k}{\partial z} = 0, \tag{21}$$

$$\lambda\theta_k + U\frac{\partial\theta_k}{\partial r} + W\frac{\partial\theta_k}{\partial z} + u_k\frac{\partial\Theta}{\partial r} + w_k\frac{\partial\Theta}{\partial z} = \frac{1}{Pr}\left(\frac{\partial^2\theta_k}{\partial r^2} + \frac{1}{r}\frac{\partial\theta_k}{\partial r} - \frac{k^2}{r^2}\theta_k + \frac{\partial^2\theta_k}{\partial z^2}\right). \tag{22}$$

The functions $\{u_k, v_k, w_k, p_k, \theta_k\}$ are Fourier coefficients which define the eigenvector of (10)–(15) for each eigenvalue $\lambda(k)$. The integer number k in (17) plays a role of the azimuthal wavenumber. The value $k=0$ corresponds to the axisymmetric perturbation.

It is seen that the linear stability problem can be solved separately for each value of the azimuthal wavenumber k. This allows us to replace the full three-dimensional stability problem by a series of axisymmetric problems for different azimuthal wavenumbers k.

The main problem of numerical solution of the system (18)–(22) is caused by the terms proportional to $1/r^2$, which lead to a non-integrable discontinuity at the axis of the cylinder $r=0$. Note that this discontinuity is an artifact introduced by the use of polar coordinates in the (r,φ) plane. However, this artificial discontinuity can be easily avoided. Note, that the azimuthal angle φ is not defined at $r=0$. This means that a non-zero value of each function can be assigned at $r=0$ to one of the Fourier modes, while all the other modes can be put equal to zero at the axis. Hence, it follows for Eqs. (20) and (22), that non-zero values of the axial velocity and the temperature should be assigned to the axisymmetric mode $k=0$. To do the same for Eqs. (18) and (19), one can express the terms $(2iku_k/r^2)$ and $(2ikv_k/r^2)$ from the continuity equation (21) as

$$\frac{2ik}{r^2}u_k = -\frac{2ik}{r}\left(\frac{\partial u_k}{\partial r} + \frac{ik}{r}v_k + \frac{\partial w_k}{\partial z}\right), \qquad \frac{2ik}{r^2}v_k = -\frac{2}{r}\left(\frac{\partial u_k}{\partial r} + \frac{u_k}{r} + \frac{\partial w_k}{\partial z}\right) \tag{23}$$

and substitute (23) into (18) and (19), which gives

$$\lambda u_k + U\frac{\partial u_k}{\partial r} + W\frac{\partial u_k}{\partial z} + u_k\frac{\partial U}{\partial r} + w_k\frac{\partial U}{\partial z} = -\frac{\partial p_k}{\partial r} + \frac{1}{Re}\left(\frac{\partial^2 u_k}{\partial r^2} + \frac{3}{r}\frac{\partial u_k}{\partial r} - \frac{k^2-1}{r^2}u_k + \frac{\partial^2 u_k}{\partial z^2} + \frac{2}{r}\frac{\partial w_k}{\partial z}\right), \tag{24}$$

$$\lambda v_k + U\frac{\partial v_k}{\partial r} + W\frac{\partial v_k}{\partial z} - \frac{Uv_k}{r} = -ikp_k + \frac{1}{Re}\left(\frac{\partial^2 v_k}{\partial r^2} + \frac{1}{r}\frac{\partial v_k}{\partial r} + \frac{k^2-1}{r^2}v_k + \frac{\partial^2 v_k}{\partial z^2} - \frac{2ik}{r}\frac{\partial u_k}{\partial r} - \frac{2ik}{r}\frac{\partial w_k}{\partial z}\right). \tag{25}$$

It is easy to see now, that terms proportional to $1/r^2$ disappear at $k=1$. This gives us a possibility to assign non-zero values of u and v at $r=0$ to the Fourier components corresponding to $k=\pm 1$. Finally, we obtain the following restrictions for

values of the Fourier modes at $r=0$:

$$u_0 = 0,\ v_0 = 0,\ \theta_0 \neq 0,\ w_0 \neq 0,$$
$$u_{\pm 1} \neq 0,\ v_{\pm 1} \neq 0,\ w_{\pm 1} = \theta_{\pm 1} = 0, \tag{26a}$$

$$u_k = v_k = w_k = \theta_k = 0, \quad \text{for } |k| > 1. \tag{26b}$$

NUMERICAL METHOD

The axisymmetric problem (6)–(9) together with the three-dimensional linear stability problem (18)–(22) are solved using the spectral Galerkin method, as described in detail in G. Here we shall outline some the main steps.

The system of basis functions of the Galerkin method is divided into axisymmetric and asymmetric subsystems. This allows us to extract the axisymmetric problem for the basis flow as a separate part and then consider only a three-dimensional stability problem. Furthermore, it follows from the continuity equation (21), that among the three systems of basis functions for u_k, v_k and w_k only two will be linearly independent. Taking this into account, the resulting Galerkin expansion of the velocity can be written as follows:

$$\mathbf{v} = \sum_{i=1}^{M_r}\sum_{j=1}^{M_z} A_{ij}\,\mathbf{U}_{ij}(r,z) + \sum_{k=-\infty}^{k=\infty}\left\{\sum_{i=1}^{N_r}\sum_{j=1}^{N_z}\left[B_{ij}^k\,\mathbf{V}_{ij}(r,z) + C_{ij}^k\,\mathbf{W}_{ij}(r,z)\right]\right\} \times \exp(\mathrm{i}k\varphi), \tag{27}$$

where, A_{ij}, B_{ij}^k and C_{ij}^k and are unknown coefficients. The vector functions $\mathbf{U}_{ij}$ form the basis of the axisymmetric part ($k=0$) of the 3D flow in the (r,z) plane. The vector functions $\mathbf{V}_{ij}$ and $\mathbf{W}_{ij}$ form bases for the remaining part of the three-dimensional flow in the (r,φ) and (z,φ) coordinate surfaces respectively. Components of the basis functions, normal to the corresponding coordinate surfaces, vanish: $U_{ij}^{(\varphi)} = V_{ij}^{(z)} = W_{ij}^{(r)} = 0$. Components of the basis functions $\mathbf{U}_{ij}$, $\mathbf{V}_{ij}$ and $\mathbf{W}_{ij}$ are defined as linear superpositions of Chebyshev polynomials as follows:

$$\mathbf{U}_{ij} = \begin{bmatrix} (r/2)\sum_{l=0}^4 a_{il}T_{i+l}(r)\sum_{l=0}^4 b_{jl}U_{j+l-1}(z/A) \\ 0 \\ -\sum_{l=0}^4 a_{il}\tilde{U}_{i+l-1}(r)\sum_{l=0}^4 (b_{jl}/2(j+l))T_{j+l}(z/A) \end{bmatrix}, \tag{28}$$

$$\mathbf{V}_{ij} = \begin{bmatrix} -ikr^\alpha \sum_{l=0}^4 c_{il}T_{i+l}(r)\sum_{l=0}^4 d_{jl}T_{j+l}(z/A) \\ \sum_{l=0}^4 c_{il}\hat{U}_{i+l}(r)\sum_{l=0}^4 d_{jl}T_{j+l}(z/A) \\ 0 \end{bmatrix}, \tag{29}$$

$$\mathbf{W}_{ij} = \begin{bmatrix} 0 \\ r^2\sum_{l=0}^4 e_{il}T_{i+l}(r)\sum_{l=0}^4 f_{jl}U_{j+l-1}(z/A) \\ -ikr\sum_{l=0}^4 e_{il}T_{i+l}(r)\sum_{l=0}^4 (f_{jl}/2(j+l))T_{j+l}(z/A) \end{bmatrix}. \tag{30}$$

Here $\alpha=0$ for $|k|=1$ and $\alpha=1$ for $|k|>1$, T_i and U_j are the Chebyshev polynomials of the 1st and the 2nd kind, and

$$\tilde{U}_n(r) = T_{n+1}(r) + (n+1)rU_n(r),$$
$$\hat{U}_n(r) = (\alpha+1)r^\alpha T_n(r) + 2nr^{\alpha+1}U_{n-1}(r). \tag{31}$$

The coefficients a_{il}, b_{jl}, e_{il}, f_{jl} are used to satisfy all the boundary conditions. Because of the relation between the Chebyshev polynomials

$$\frac{\mathrm{d}}{\mathrm{d}x}T_{n+1}(x) = 2(n+1)U_n(x), \tag{32}$$

the basis functions (28)–(30) are analytically divergence-free. If there is no flow through the boundaries of the flow region, the projection of the pressure gradient on a solenoidal basis function yields

$$\int_V \nabla p\cdot\mathbf{U}_{ij}\,\mathrm{d}V = \int_V \nabla p\cdot\mathbf{V}_{ij}\,\mathrm{d}V = \int_V \nabla p\cdot\mathbf{W}_{ij}\,\mathrm{d}V = 0. \tag{33}$$

Therefore, there is no need to determine the pressure if a solenoidal basis, satisfying no-throughflow boundary conditions, is used for the global Galerkin method. All terms containing Fourier modes of the pressure p_k vanish after projection of the Eqs. (18)–(22) on the solenoidal bases (28)–(30).

For the temperature (or other transported scalar property) the Galerkin expansion can be written as follows:

$$\theta = G(r,z) + \sum_{k=-\infty}^{k=\infty} \left\{ q(k,r) \sum_{i=0}^{N_r} \sum_{j=0}^{N_z} D_{ij}^{k} \sum_{l=0}^{2} \sigma_{il} T_{i+l}(r) \times \sum_{m=0}^{2} \delta_{jm} T_{j+m}\left(\frac{z}{A}\right) \right\} \exp(ik\varphi), \quad (34)$$

$$q(k,r) = ikr, \quad \text{if } k \neq 0; \quad q(0,r) = 1.$$

The coefficients σ_{il} and δ_{jm} are used to satisfy the homogeneous boundary conditions (15). The function $G(r,z)$ is used to satisfy non-homogeneous boundary conditions for the temperature also expressed as a series of the Chebyshev polynomials

$$G(r,z) = \sum_{i=0}^{N_r} \sum_{j=0}^{N_z} g_{ij} T_i(r) T_j\left(\frac{z}{A}\right). \quad (34^*)$$

This approach was used in G to analyze the *axisymmetric* instabilities of a basic *rotating* flow. Here we use a similar technique for the *non-axisymmetric* instability of a basic *non-rotating* flow. Further details of the numerical solution follow the same steps as in G. The results are given in the following.

Test Calculations

The first test case considered was the Rayleigh–Benard instability of motionless fluid in a cylinder heated from below. Comparison with other results for a stationary cylinder (Hardin *et al.*, 1990) and for a cylinder rotating around its axis (Jones and Moore, 1979; Goldstein *et al.*, 1993) showed that the calculated critical Rayleigh number is correct up to the fifth digit with the use of 10×10 basis functions in the r- and z-directions. Details may be found in Gelfgat and Tanasawa (1993). However, these tests are not sufficient, because the convective terms of the momentum equation vanish in the case of motionless initial state.

The next test case considered was the onset of the secondary, oscillatory instability of the axisymmetric Rayleigh–Benard convective flow. A cylinder with isothermal top and bottom and perfectly insulated lateral wall was considered. For aspect ratio equal to 1, the axisymmetry-breaking bifurcation sets in as a transition to steady 3D flow with the azimuthal number $k = 2$. An illustration of the convergence of the critical Rayleigh number ($Ra = GrPr$) and a comparison with recent results of Wanschura *et al.* (1996) are shown in Table I.

A hysteresis of Ra_{cr} at $k = 2$ was found by Wanschura *et al.* (1996) for $Pr = 1$. With the increase of Ra the axisymmetric flow becomes unstable with respect to asymmetric perturbations at a certain value $Ra_{cr}^{(1)}$ and then, with further increase of the Rayleigh number, it becomes stable at a larger value $Ra_{cr}^{(2)} > Ra_{cr}^{(1)}$. This result was used as another test, and was extended further: the third value $Ra_{cr}^{(3)} > Ra_{cr}^{(2)}$ at which the steady axisymmetric flow becomes finally unstable was also calculated. The convergence of all three critical Rayleigh numbers is shown in Table II.

TABLE I Critical Rayleigh number for the azimuthal mode $k = 2$

$N_r \times N_z$	$Pr = 0.02$	$Pr = 1$
6×6	2493.74	3003
10×10	2493.72	3004
20×20	2493.72	3004
Wanschura *et al.* (1996)	2463	3016
Neumann (1990)	2525	—

TABLE II First, second, and third critical Rayleigh numbers for $Pr = 1$, $A = 1$, $k = 2$

$N_r \times N_z$	$Ra_{cr}^{(1)}$	$Ra_{cr}^{(2)}$	$Ra_{cr}^{(3)}$
10×10	3004	7841	25924
20×20	3004	7842	25945
30×30	3004	7842	25945
Wanschura *et al.* (1996)	3016	7900	

Further tests of convergence of Ra_{cr} and ω_{cr} were made for $A = 1$, $Pr = 0.02$ and 1.0, and mode wavenumbers $k = 0, 1, 2, 3, 4$, and 5, with numbers of basis functions running from 6×6, $8 \times 8, \ldots$, to 28×28, 30×30. For all parameter values except $Pr = 0.02, k = 0$, the values of Ra_{cr} and ω_{cr} converged to four or five significant digits from 14×14 functions on. For $Pr = 0.02$, $k = 0$ convergence was slightly slower and was reached from 28×28 functions on. The final converged results are shown in Tables III(a)–(c). Apart from the issue of convergence testing, it can be seen that the value of Ra_{cr} for $k = 2$ is lower than that for other k, for both $Pr = 1$ and $Pr = 0.02$, i.e., the $k = 2$ mode is the most unstable. Furthermore, it is interesting to observe (Table III(c)) that at low Pr the value of Ra_{cr} is quite strongly dependent on Pr.

EXPERIMENT

The onset of convection and the stability of an initially isothermal fluid in regular cavities instantaneously cooled from above have been extensively investigated for water, both with and without phase change (see KC). A sketch of the experimental setup is shown in Fig. 1. A cylinder (37.1 mm inner diameter by 41 mm inner height) filled with water was immersed in a thermostatic water bath held at a hot temperature and was closed on its top by a metal plate held at a cold temperature. The walls of the cylinder (side and bottom) were made of 2.1 mm thick glass. Experiments were carried out at bath temperatures in the range $\theta_{hot} = 10$–$25°C$ and top plate temperature cold, ranging from slightly below the bath temperature, viz., $\theta_{cold} = 20°C$, down to below the freezing point, viz., $\theta_{cold} = -10°C$. In all situations the thermal stratification resulted in a free convective flow, and for below-freezing lid temperature an ice front formed and grew downward from the top. A steady state flow configuration consists of a single cold downward jet along the cavity axis and a reverse upward flow along the side wall.

Observations were made mainly by careful and detailed measurements of the temperatures and tracks of liquid crystal tracers, at various vertical and horizontal cross-sections. The color change of the tracers convected by the flow allowed us to detect variations of the thermal field as small as 0.1°C, providing a direct indication of the stability and structure of the investigated flow field. Details of the experimental procedure and extensive results are

TABLE III Critical Rayleigh numbers for various azimuthal modes k, and various Prandtl numbers using 30×30 basis functions

k	Ra_{cr}	ω_{cr}
(a) $Pr = 1$		
0	28469	0
1	4202*	0
2	3004	0
3	23851	11.043
4	17610	0
5	17392	0
(b) $Pr = 0.02$		
0	17442	247.1
1	2662.82	0
2	2493.72	0
3	3313.9	0
4	4908.06	0
5	7406.92	0
(c) $k = 2$		
0.19	2625	0
0.2	2493.72	0
0.21	2242	0

*Compare with Neumann (1990) $Ra_{cr} = 4100$ and Wanschura *et al.* (1996) $Ra_{cr} = 4224$.

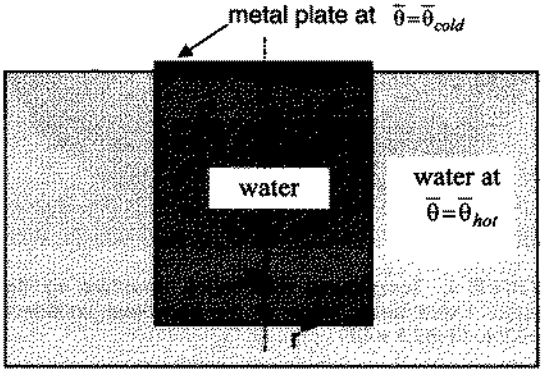

FIGURE 1 Sketch of the experimental setup. Glass cylinder with a cooled lid immersed in a hot bath.

given elsewhere (see KC, also Kowalewski *et al.*, 1998). Insofar as the present study is concerned, the interesting observation was that at a certain set of parameters the temperature field measured in the fluid in a horizontal cross-section slightly below the top ($z=0.9A$) split into a pattern of 16–18[1] wedge-like sectors extending radially from the axis to the circumference (Fig. 2). Thus, despite the cylindrical geometry the flow underneath the lid became divided into a regular pattern of radial structures. Clearly, the basic axisymmetric flow split into a non-axisymmetric (but quite regular) flow with this high wavenumber. These structures appeared for pure water convection for temperature differences $\Delta\theta = \theta_{hot} - \theta_{cold}$ exceeding 5°C. The corresponding Grashof number is $Gr = 2.46 \times 10^4$. At larger temperature difference ($\Delta\theta > 10$°C) the flow structure became unstable and the vertical "cold jet" started to bounce. The previously regular "star-like" horizontal structure of 16–18 spikes became disturbed, their number and length varied in time.

It is worth noting, that the observed flow pattern remains when the phase change takes place (freezing of water for $\theta_{cold} = -10$°C). The characteristic star-like grooves were well visible in the ice surface growing under the lid.

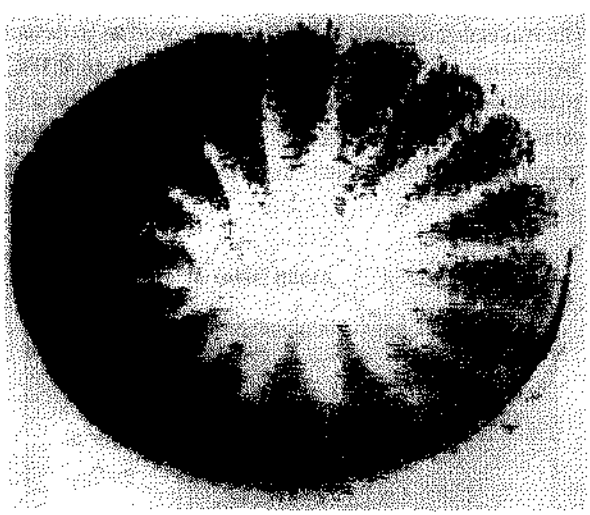

FIGURE 2 Temperature distribution visualized by liquid crystals. Color image taken at the horizontal cross-section $z=0.9A$, $Gr \approx 2.5 \times 10^4$.

NUMERICAL COMPARISON WITH EXPERIMENT

In view of the experimental observation, the further thrust of the present analytical study was to analyze numerically the splitting of axisymmetry of this flow.

A secondary, but non-trivial, problem arose in connection with the definition of the thermal boundary conditions: In a naive, first-sight description, the system appears to be defined as isothermal cold top and isothermal hot sidewall and bottom. However, as pointed out by KC, the conduction through the glass wall is finite (i.e., the inner wall surface is neither isothermal nor perfectly insulated) and there are significant temperature gradients near the upper corner, where the top plate meets the cylinder wall. To account for this effect, two different approaches were taken for the definition of the thermal boundary conditions:

(a) the boundary conditions at the inner walls were assumed to be:

$$\frac{\partial\theta}{\partial z} = -Bi(\theta - 1) \text{ at } z=0; \quad \theta = 0, \text{ at } z = A; \qquad (35)$$

$$\frac{\partial\theta}{\partial r} = Bi\left(\theta - \left[1 - \left(\frac{z}{A}\right)^n\right]\right) \qquad \text{at } r = 1, \qquad (36)$$

and no-slip conditions for the velocity on all boundaries. Here $\theta = (\bar{\theta} - \bar{\theta}_{cold})/(\bar{\theta}_{hot} - \bar{\theta}_{cold})$, Bi is a *semi-artificial* Biot number, and the power function $(z/A)^n$ with the *artificial* exponent n is added to smoothen the temperature boundary conditions at the top edge of the cylinder;

(b) the *compound* problem of *axisymmetric* convection in the cylinder with *finite conduction* through the walls was computed by a finite-volume method (the isothermal conditions were assumed

[1] The shape of the wedges was not perfectly uniform. A simple count gave 17. The correct number could be either 17 or the nearest even numbers 16 or 18.

on the *outside* of the walls). Then the resulting temperature distribution on the inner walls was taken as boundary condition for the non-axisymmetric stability analysis.

The details of the two approaches and the results are described below.

"Artificial" *Bi* and *n*

As stated above, the thermal boundary condition at the inner walls was approximated by assuming (35) and (36). With these boundary conditions, the function $G(r, z)$ in (34) was chosen as

$$G(r,z) = \left[1 - \left(\frac{z}{A}\right)^n\right] + \left[1 + \frac{Bi}{2+Bi} r^2\right] \left(\frac{z}{A}\right)^n \left(1 - \frac{z}{A}\right). \quad (37)$$

The Biot number *Bi* and the exponent *n* depend on heat transfer between the metal plate, the thermostatic bath, and the entire enclosure. Unfortunately, there is not enough experimental data to determine accurate values of these parameters. Therefore, *Bi* and *n* were varied with the goal to find whether there exists a most dominant 3D perturbation which is divided into 18 similar parts in the azimuthal direction.

A coarse estimate of the Biot number may be obtained from the balance of the heat flux at the inner and outer boundary of the cylindrical wall. Assuming that the heat transfer coefficient from the wall to the outer water bath is about 10^3 W/m^{2}K and that the heat conductivities of glass and water are 1.02 and 0.566 W/mK, respectively, the estimate is $Bi \approx 10$. In the following calculations the Biot number was varied from 0.5 to 20.

Preliminary calculations were done with the exponent $n = 20$ in (37). (All computational results presented from here on are for $A = H/R = 2.2$ and $Pr = 8.0$, which correspond to the parameters of the experiments.) The dependence of the critical Grashof number on the azimuthal number k for different values of *Bi* is shown in Fig. 3. At $Bi = 20$

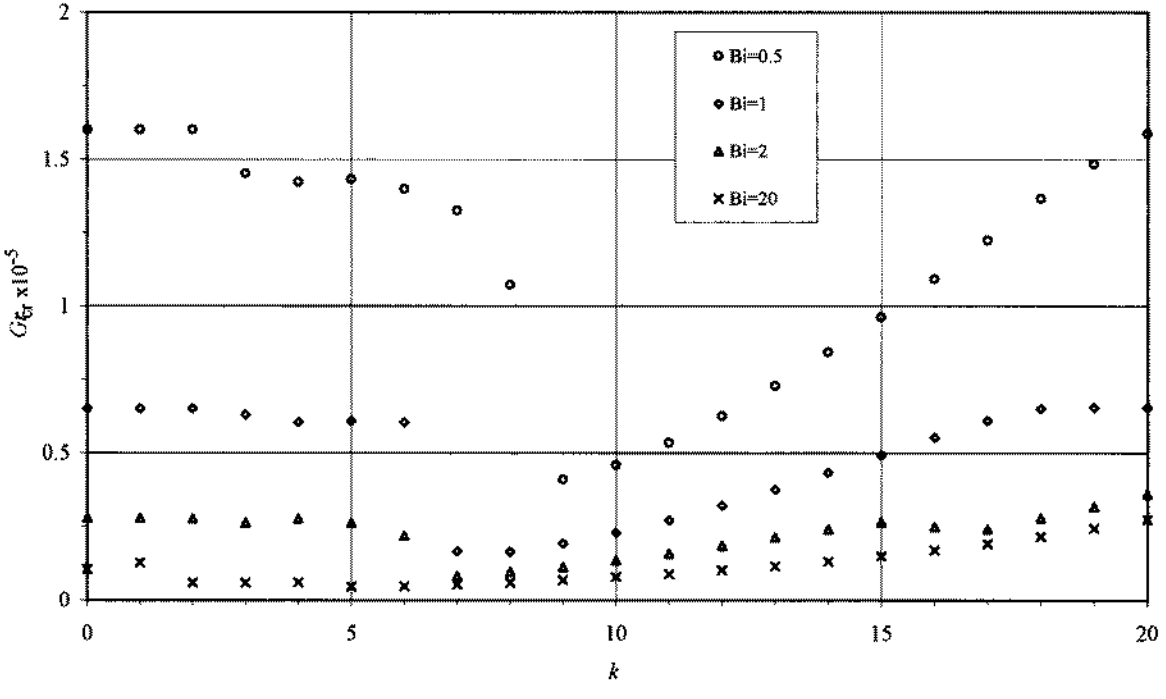

FIGURE 3 Critical Grashof number Gr_{cr} corresponding to different azimuthal wavenumbers k for $n = 20$ in (36).

the minimum $Gr_{cr}(k)$ corresponds to the dominant azimuthal mode with $k=5$. With the decrease of Bi the number of the dominant azimuthal mode grows. At $Bi=2$ there is an abrupt decrease to the dominant azimuthal mode $k=7$ from the mode $k=6$ (Fig. 3). With further decrease of the Biot number this abrupt decrease becomes larger and occurs at larger k. At $Bi=0.5$ the most unstable azimuthal mode is $k=9$.

The axisymmetric convective flow for $Bi=0.5$ and $n=20$ is shown in Fig. 4 for the critical Grashof number corresponding to $k=9$. Figure 5 shows the corresponding dominant three-dimensional *perturbation* of the temperature whose azimuthal period is $2\pi/9$. Figures 6 and 7 illustrate the same but for $Bi=20$ and $k=5$. Note, that the most unstable perturbation (Figs. 5 and 7) consists of a pair of antisymmetric patterns which are separated by a plane $\varphi=const$. The perturbation of the three-dimensional velocity is similar.

A comparison of the dominant perturbation (Figs. 5 and 7) with the distribution of the temperature in the mean axisymmetric flow (Figs. 4 and 6) allows us to make some conclusions about the nature of the instability. It is seen that an unstably stratified fluid layer is always located near the upper cold plate. The depth of the layer depends on the Biot number and on the smoothing of the temperature at the upper edge (the exponent n). The maximal absolute values of the perturbation of the temperature are also located near the upper plate. The patterns of the perturbation of the vector potential of velocity ($\Psi^{(r)}$ and $\Psi^{(z)}$, not shown in the paper) also look similar. This

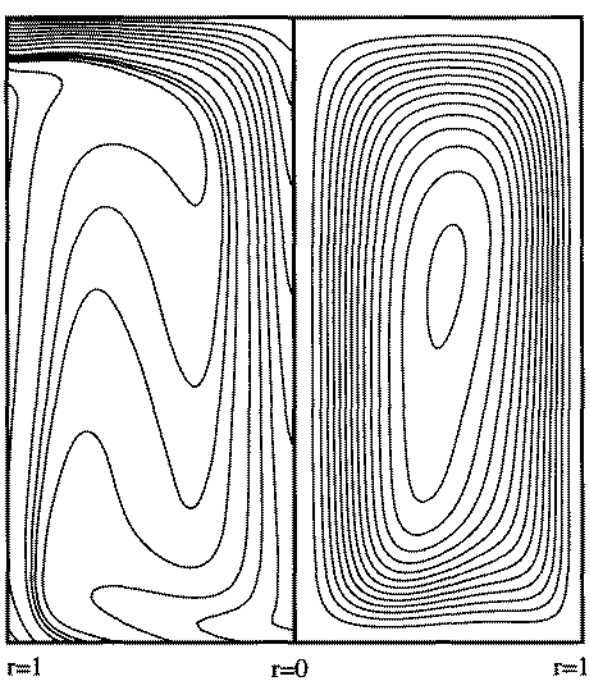

FIGURE 4 Streamlines and isotherms of the *axisymmetric* flow $Bi=0.5$, $n=20$, $Gr=Gr_{cr}=40{,}900$.

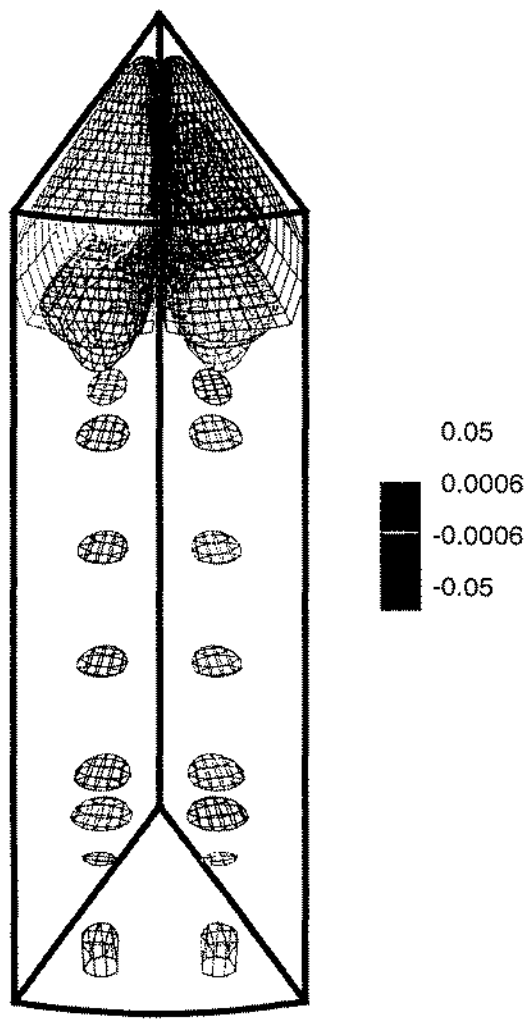

FIGURE 5 Isosurfaces of the 3D *perturbation* of the temperature. $Bi=0.5$, $n=20$, $k=9$, $Gr=Gr_{cr}=40{,}900$.

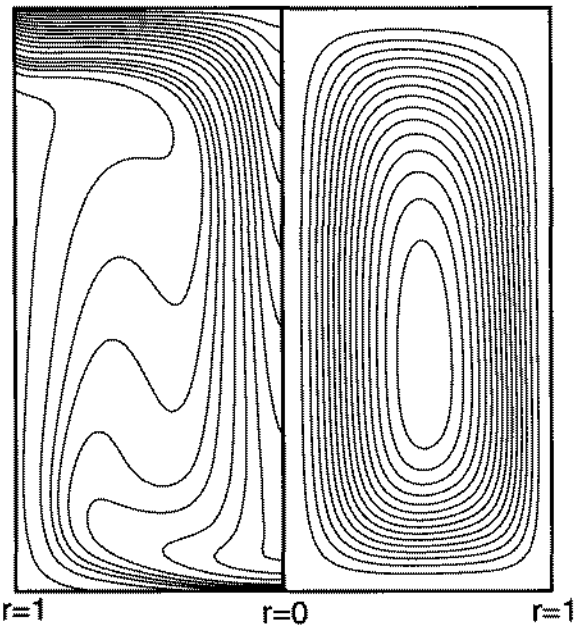

FIGURE 6 Streamlines and isotherms of the *axisymmetric* flow $Bi = 20$, $n = 20$, $Gr = Gr_{cr} = 4600$.

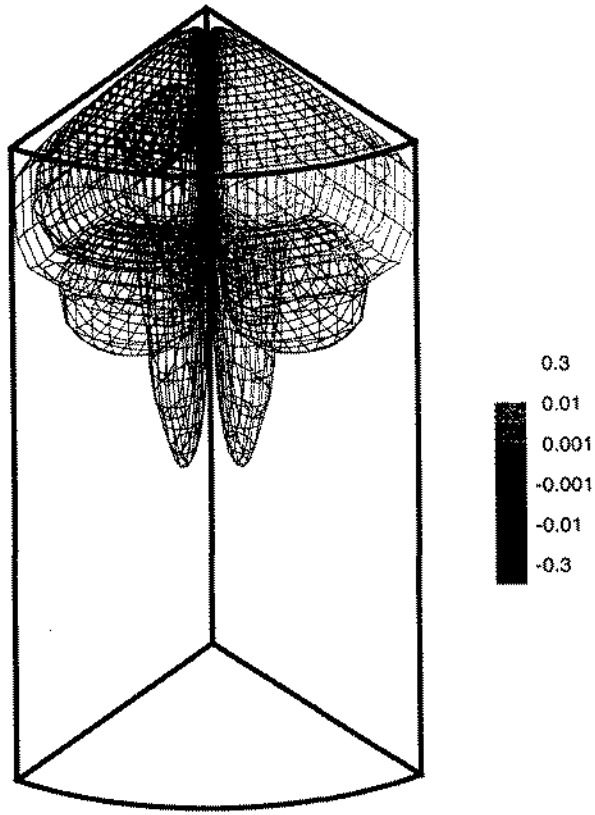

FIGURE 7 Isosurfaces of the 3D *perturbation* of the temperature. $Bi = 20$, $n = 20$, $k = 5$, $Gr = Gr_{cr} = 4600$.

allows us to conjecture that the observed instability is caused by a Rayleigh–Benard mechanism in the unstably stratified fluid layer.

Maximal values of the perturbation appear on surfaces which have almost rectangular cross section at the cylindrical wall (Figs. 5 and 7). The size of these "rectangles" grows with the growth of the depths of the stratified layers. This means that for thinner layers the size of the characteristic patterns of the most unstable perturbation will be smaller and the corresponding critical azimuthal number will be larger (the length of each "rectangle" in the circumferential direction is π/k).

The depth of the unstably stratified fluid layer strongly depends on the heat transfer conditions in the vicinity of the upper edge of the cylinder. Quantitative comparison with the experiment is hardly possible without better approximation of these conditions in the calculations (see below, Finite Wall Conduction Analysis). However, in the framework of the present numerical model it is possible to control the depth of the stratified layer by varying the exponent n in (37), which corresponds to different smoothings of the discontinuity of the temperature at the upper edge of the cylinder.

It was found that for the values of the Biot number $Bi = 10$ or 20 the instability sets in with the azimuthal number $k = 9$ if one assigns $n = 34$ in (37). This is illustrated in Figs. 8–10 for $Bi = 20$. It is seen (Fig. 8) that the critical azimuthal number grows with the growth of the exponent n, which corresponds to the thinning of the stratified layer. It is interesting to compare flow patterns with the same k but different Bi and n. Thus, compare the results for $Bi = 0.5$, $n = 20$, $Gr = 40\,900$ (Figs. 4 and 5) and for $Bi = 20$, $n = 34$, $Gr = 6770$ (Figs. 9 and 10), both of which correspond to a dominant instability with $k = 9$. The depths of the stratified layers in Figs. 4 and 9 are almost equal, which leads to the onset of instability with the same azimuthal number and with similar perturbations (compare Figs. 5

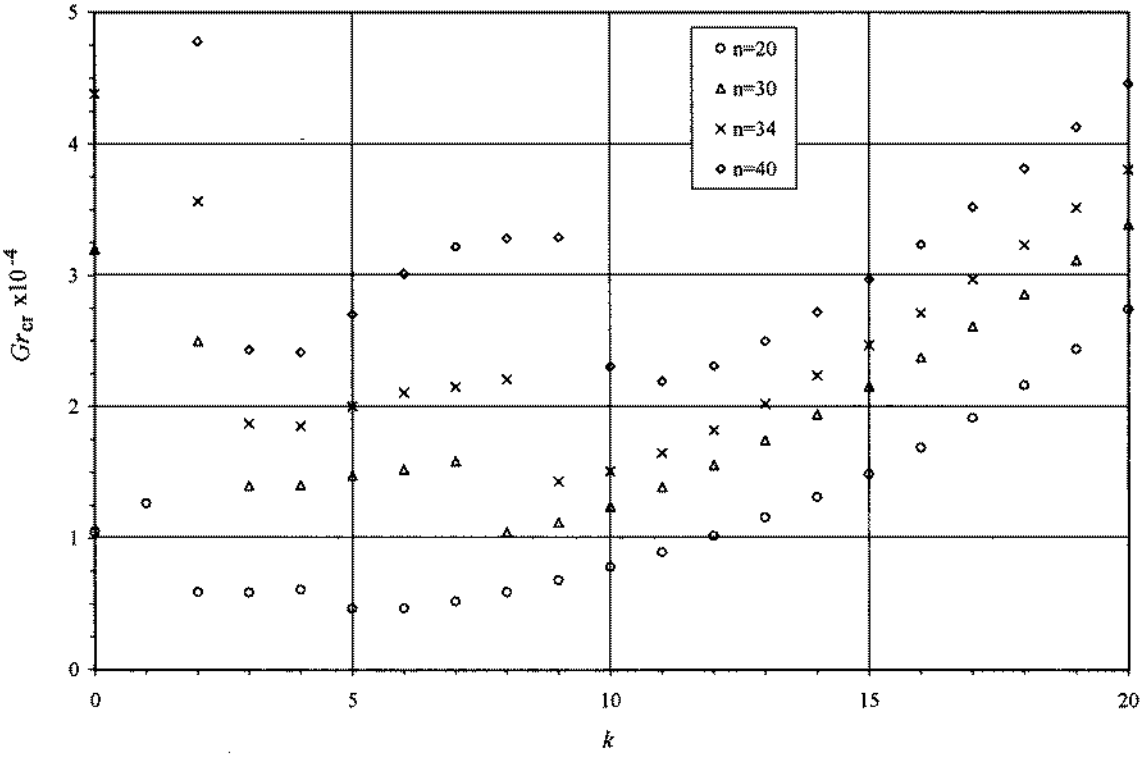

FIGURE 8 Critical Grashof number Gr_{cr} corresponding to different azimuthal numbers k for $Bi = 20$.

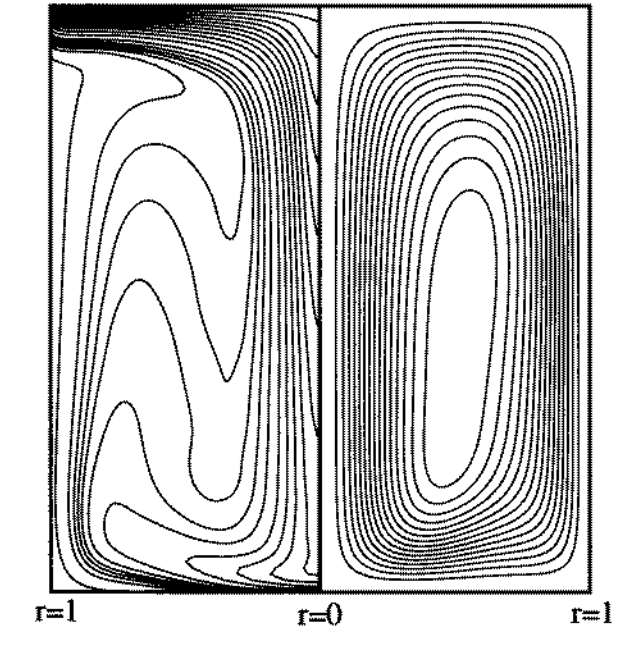

FIGURE 9 Streamlines and isotherms of the *axisymmetric* flow $Bi = 20$, $n = 34$, $k = 9$, $Gr = Gr_{cr} = 6770$.

and 10). Note, that for larger n the critical azimuthal number is larger ($k = 11$ for $n = 40$, Fig. 8). Obviously, there should be some limit of the critical k when n tends to infinity.

The results presented so far show that (a) the analysis of non-axisymmetric instability by the present Galerkin and mode-separation approach yields meaningful results and (b) for the natural convection problem considered here, the axisymmetry-breaking instability appears to be closely related to the thickness of the thermally stratified layer under the lid, nearly regardless of the specific values of parameters which led to the formation of that particular thickness.

To further investigate if the $k = 16$–18 circumferential splitting which was observed in the experiment could be obtained analytically, the computations were run for a variety of values of Bi and n. Representative results for $Gr_{cr}(k)$ for $Bi = 10$, $n = 50, 60, 70$ are shown in Fig. 11.

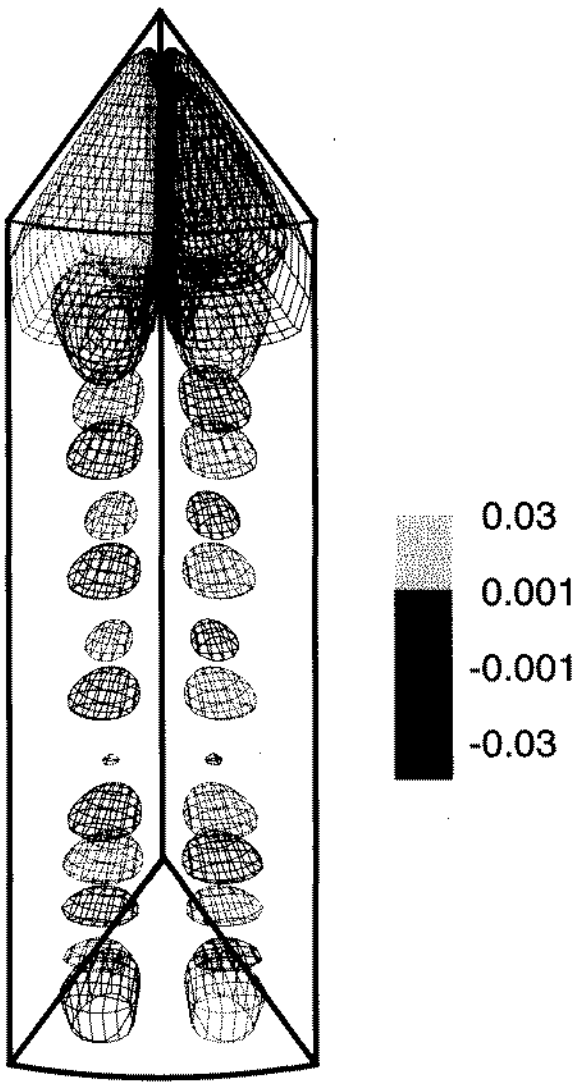

FIGURE 10 Isosurfaces of the 3D *perturbation* of the temperature. $Bi = 20$, $n = 34$, $k = 9$, $Gr = Gr_{cr} = 6770$.

The isolines of the main flow and of the perturbation are of the same nature as Figs. 4–7, 9–10 above, but more clustered near the top cover, as could be expected for the higher value of n. The behavior for the three values of n is analogous, with some shift in the characteristic values. The common result is that a *local* minimum Gr_{cr} appears at $k = 13$ ($n = 50$), $k = 14$ ($n = 60$), $k = 16$ ($n = 70$), but a *global* minimum Gr_{cr} appears near $k = \sim 4$. The question then arises why was the splitting observed at $k = 16$–18, rather than at $k = \sim 4$. The resolution of this question we hope to find in further more detailed experiments. Possibly, due to some transient effect, the instability leads to the $k = 16$–18 mode without first exhibiting the $k = \sim 4$ mode (perturbations growth rates at $Gr = 4 \times 10^4$ for $k = 4$ and 16 are of the same order of magnitude $\sim 10^1$). Alternatively, the $k = 16$–18 mode could be the result of *non-linear* interaction of lower k modes, since the value of $Gr = 2.46 \times 10^4$ in the experiment was significantly above the critical values of Gr_{cr}. In that case the observed $k = 16$–18 could be the non-linear interaction of $k = 7, 8, 9, 10$, etc.

Finite Wall Conduction Analysis

The preceding approximate description of the thermal boundary condition ("artificial" Bi and n) indicated that the stability results are, indeed, sensitive to the details. Therefore in the second approach the temperature at the inner wall was computed numerically taking into account finite conduction in the wall. (The detailed temperature distribution at the inner wall was not available experimentally. It is hoped that in future experiments this will be estimated, although the fine resolution will be difficult.) The numerical study was done in the following way: First, the coupled axisymmetric problem of convective flow inside the container and heat conduction through its walls was solved using the finite-volume method. Then the calculated profiles of the temperature at the inner surface of the side wall and the bottom were applied as the boundary conditions for the Galerkin method, such that boundary conditions for the temperature became

$$\theta = \theta_{\text{bottom}}(r) \quad \text{at } z = 0; \tag{38}$$

$$\theta = 0, \ \text{at } z = A; \quad \theta = \theta_{\text{wall}}(z) \ \text{at } r = 1, \tag{39}$$

and no-slip conditions for the velocity were imposed on all boundaries. Streamlines and isotherms of the flow calculated at $Gr = 10^4$ are illustrated in Fig. 12. Note that the temperature field extends into the walls, which are indicated by

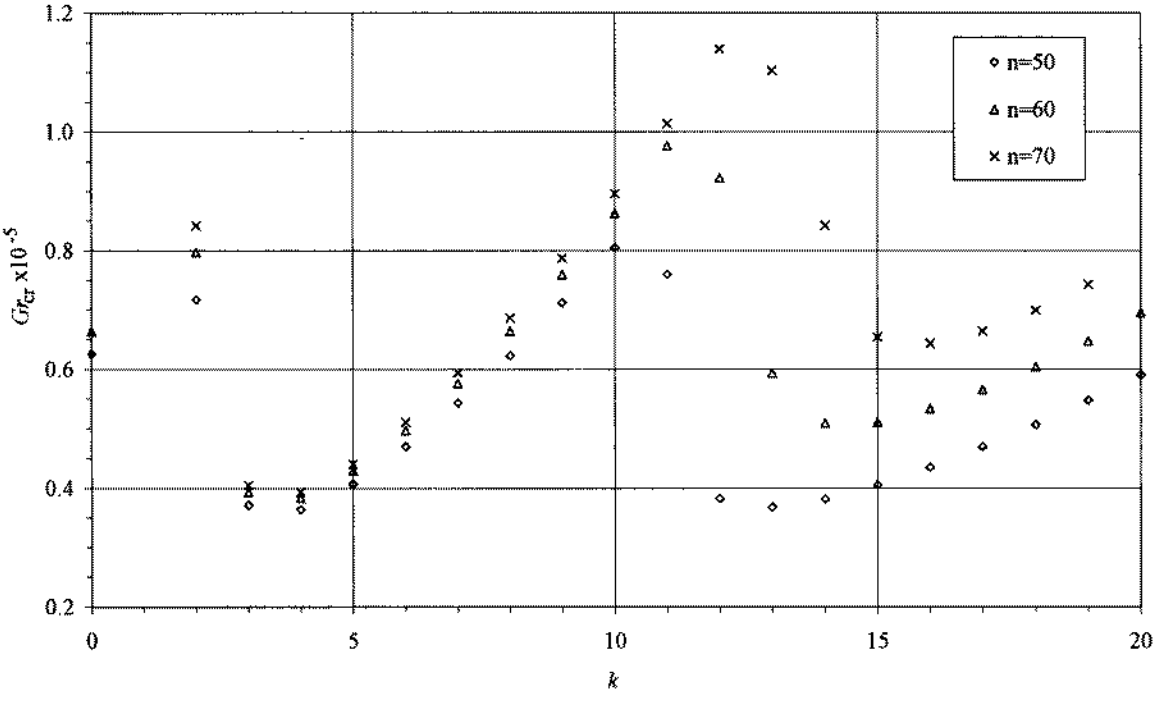

FIGURE 11 Critical Grashof number Gr_{cr} corresponding to different azimuthal numbers k for $Bi = 10$.

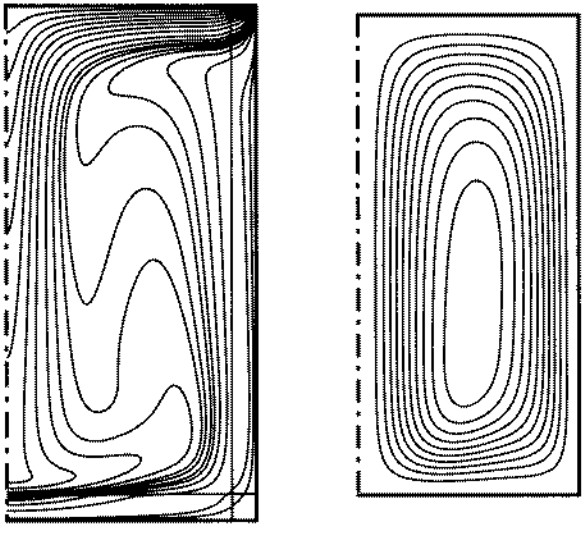

FIGURE 12 Streamlines (right) and isotherms (left) of the calculated convective flow. $Pr = 8$, $Gr = 10^4$.

the straight lines. The corresponding profiles of θ_{wall} and θ_{bottom} are shown in Fig. 13. Similar computations (not shown) were carried out for other values of Gr. The Biot number at the inner wall was computed from the numerical solution and was found to be approximately $Bi \approx 17$ at the bottom and $Bi \approx 18$ at the side wall.

With the *base flow* temperature distribution established, the stability study was carried out for three different boundary conditions for the *perturbation* of the temperature θ imposed on the side wall of the cylindrical container. One assumption was the vanishing of the perturbation of the temperature:

$$\theta = 0 \quad \text{at } r = 1. \tag{40}$$

The two other assumptions were:

$$\frac{\partial \theta}{\partial r} = Bi\theta \quad \text{at } r = 1, \tag{41}$$

where $Bi = 0$ corresponds to the vanishing of the perturbation of the heat flux on the wall and $Bi = 18$ corresponds to the calculated value of Bi.

The calculated values of the critical Grashof number Gr_{cr} for different azimuthal wavenumbers k are shown in Fig. 14. The general trend is the same

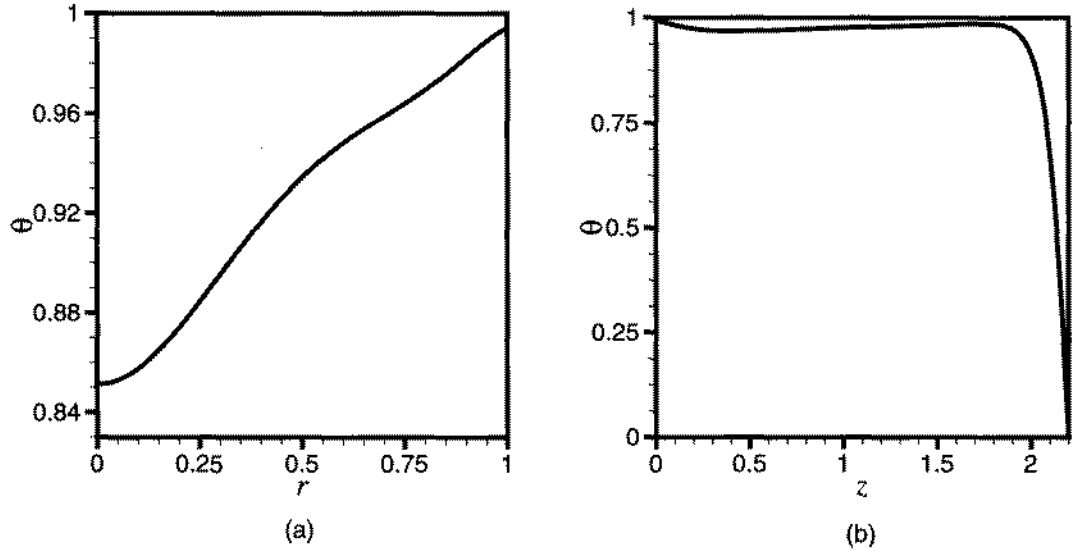

FIGURE 13 Temperature profiles calculated on the bottom (a) and the sidewall (b) of the cylindrical container. $Pr = 8$, $Gr = 10^4$.

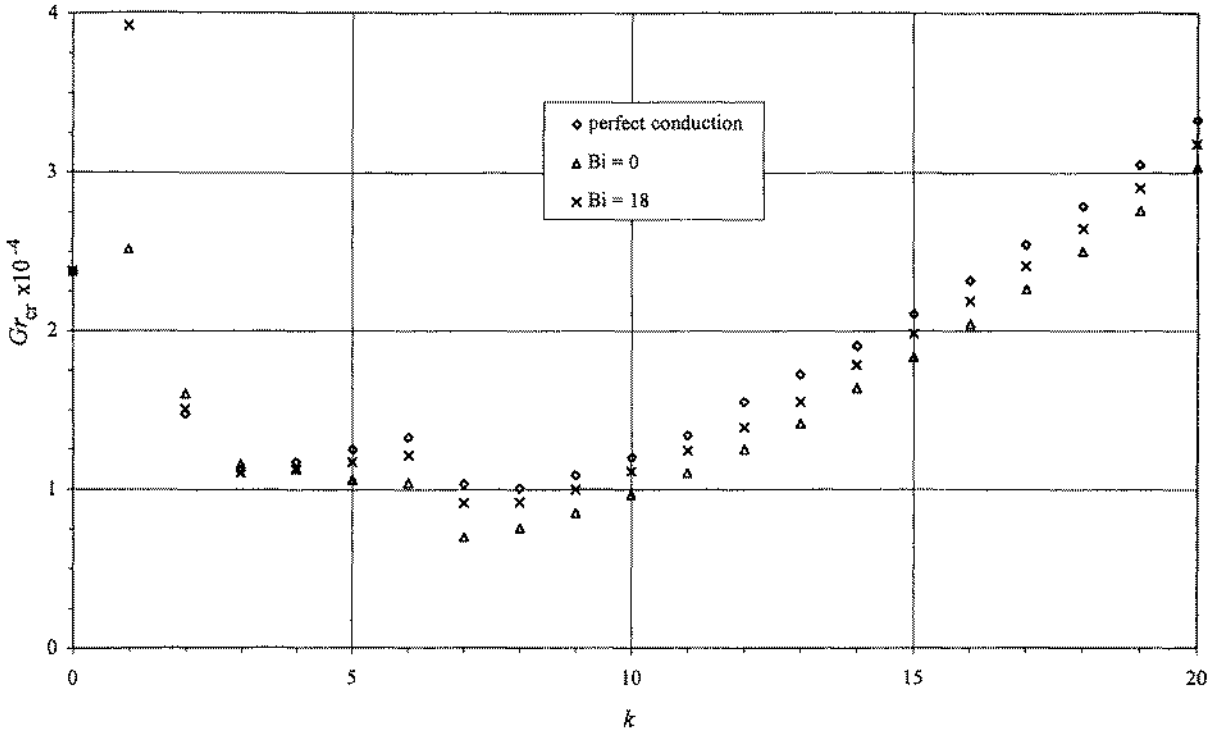

FIGURE 14 Critical Grashof number Gr_{cr} corresponding to various azimuthal wavenumbers k, for different boundary conditions for the perturbation of the temperature.

as for the other model, shown in Figs. 3 and 5. The assumed boundary conditions have some effect on the details of the results, but without altering the trend[2]. It is seen that, for all three assumptions regarding the boundary condition at the wall, the minimal values of the critical Grashof numbers correspond to $k=7$, 8 and 9 and are located close to $Gr=10^4$. An example of isolines of the perturbation of the temperature at the horizontal cross-section $z=0.9A$ (corresponding to the location of the photograph in Fig. 2) is shown in Fig. 15.

The pattern of the perturbation in this cross-section contains 8 *pairs of maxima* and *minima* (total 16 regions) and looks similar to the experimental pattern of isotherms (Fig. 2). However, the agreement with the experiment is not complete, because the dark areas in Fig. 2 correspond to the *minima* of the temperature. Therefore one should expect the existence of 16, 18 *pairs* of maxima and minima in the perturbation of the temperature.

The disagreement of the experimental and numerical results can be explained if one compares the Grashof number corresponding to Fig. 2 ($Gr=2.46\times10^4$) with the calculated critical Grashof number ($Gr_{cr}\approx10^4$). The experimental study was carried out at more than 100% supercriticality, where non-linear interaction of the dominant modes of the perturbation cannot be neglected. Thus, the 17 minima of the temperature, seen in Fig. 2, can be a result of non-linear interaction of modes with $k=8$ and 9, or $k=7$ and 10, whose critical Grashof numbers have close values. On the other hand, modes with $k=16, 18$ also become unstable at $Gr\approx2.5\times10^4$, and can become dominant at certain conditions.

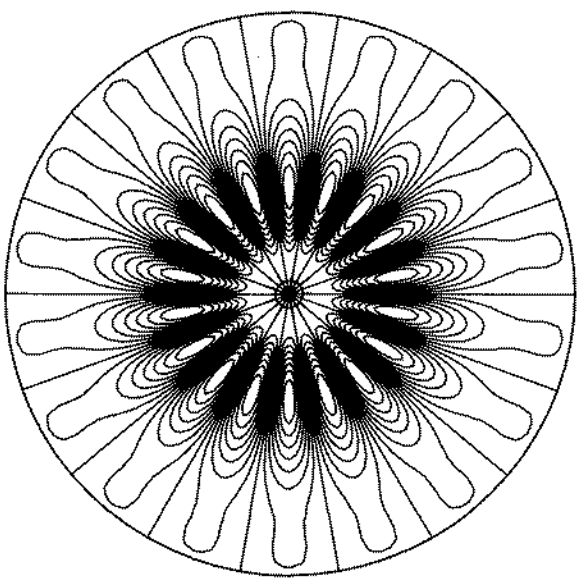

FIGURE 15 Isolines of perturbation of temperature at the cross-section $z=0.9A$. Case of vanishing temperature perturbation at side wall. $Gr_{cr}=1.01\times10^4$, $k=8$.

CONCLUSIONS

It was shown that the global spectral approach may be successfully applied to numerical studies of axisymmetry-breaking instabilities. Using this approach, one can consider a linearized 2-D stability problem for each circumferential mode separately, instead of CPU-time-consuming, time-dependent calculations. The proposed spectral approach was validated by comparison with the results of direct numerical simulation. (This approach is also used to analyze the stability of *rotating* flows, which will be reported elsewhere.)

The use of the global spectral approach allowed us to obtain a qualitative explanation of the recently reported experimental results (KC) for natural convection in a cylindrical container, in which an instability with a relatively high azimuthal number ($k=16\div18$) was observed. The spectral Galerkin analysis presented here reproduces such instabilities and provides details of the flow and temperature

[2] Our experiments also included an investigation in which a slightly insulated ring of 4 mm height (adhesive tape) was wrapped on the outside of the cylinder just below the cold cover, thus smoothing the temperature discontinuity. We have reproduced this situation in the computations (not shown). The general trend of the instability is still the same, with some differences in detail. Further comparison of experiment and computation for this situation will be meaningful only when detailed measurements of the temperature in the transition region become available.

field. In the absence of detailed experimental data on the temperature distribution in the critical region near the upper corner, various approximations were assumed, all leading to a splitting of axisymmetry with high to very high circumferential wavenumber. The non-simple thermal boundary conditions of the experiments were approximated in several ways, including a hybrid numerical approach, in which the base flow was computed taking into account wall conduction, and the results were used to define thermal boundary conditions for the 3-D stability problem.

The numerical results support the conjecture of KC that the instability is of Rayleigh–Benard type, generated by the thermal stratification near the upper corner of the cylinder. The analysis predicts a high azimuthal number close to that observed in experiment. A more precise quantitative comparison with the experimental results would require better resolution of the experimental heat transfer conditions. This may suggest the line of future experimental work.

Acknowledgments

This work was supported by the Israel Science Foundation under Grant 110/96, by the Center for Absorption in Science, Israel Ministry of Immigrant Absorption (to A. Gelfgat), by the Fund for the Promotion of Research at Technion (to P. Bar-Yoseph), by the Y. Winograd Chair of Fluid Mechanics and Heat Transfer, and by the Israel High Performance Computer Unit. The fourth author would like to acknowledge the contribution of W. Hiller and C. Soeller from Max Plank Institute for Fluid Mechanics Research, Göttingen, with whom the experimental study was initiated.

NOMENCLATURE

A	aspect ratio (height/radius) of the cylinder
Bi	Biot number
Gr	Grashof number
H	height of the cylindrical cavity
Pr	Prandtl number
R	radius of the cylindrical cavity
Ra	Rayleigh number
$T_i(x)$	Chebyshev polynomial of the first kind
$U_i(x)$	Chebyshev polynomial of the second kind
g	gravity acceleration
k	azimuthal number
p	pressure
r, φ, z	cylindrical coordinates
t	time
$\mathbf{v} = (u, v, w)$	velocity vector in cylindrical coordinate system
Ψ	vector potential of velocity
β	thermal expansion coefficient
ν	kinematic viscosity
χ	thermal diffusivity
θ	temperature

References

Gelfgat, A.Yu. and Tanasawa, I. (1993) Systems of basi functions for calculation of three-dimensional fluid flows i cylindrical containers with the spectral Galerkin methoc *Journal of Institute of Industrial Science, University of Tokyo* **45**, 60–63.

Gelfgat, A.Yu., Bar-Yoseph, P.Z. and Solan, A. (1996) Stabilit of confined swirling flow with and without vortex breakdow *Journal of Fluid Mechanics*, **311**, 1–36.

Gelfgat, A.Yu., Bar-Yoseph, P.Z. and Solan, A. (1997 Axisymmetry-breaking instabilities of axially symmetric con vective flows. *Proc. 10th Intl. Conf. on Transport Phenomena i Thermal Science and Process Engineering*. Kyoto, Decembe 1997, Vol. 1, pp. 263–268.

Gelfgat, A.Yu., Bar-Yoseph, P.Z. and Solan, A. (1998) Stabilit of axisymmetric convective flows with respect to three dimensional perturbations, *Proc. 27th Israel Conference o Mechanical Engineering*, Haifa, May, 1998, pp. 315–317.

Goldstein, H.F., Knobloch, E., Mercader, I. and Net, M. (199 Convection in rotating cylinder. Part 1. Linear theory fo moderate Prandtl numbers, *Journal of Fluid Mechanics*, **24** 583–604.

Hardin, G.R., Sani, R.L., Henry, D. and Roux, B. (199(Buoyancy-driven instability in a vertical cylinder: Binar fluids with Soret effect. Part 1. General theory and stationar stability results, *International Journal for Numerical Metho in Fluids*, **10**, 79–117.

Jones, C.A. and Moore, D.R. (1979) The stability of axisym metric convection, *Geophysical and Astrophysical Flui Dynamics*, **11**, 245–270.

Kowalewski, T. and Cybulski, A. (1997) Konwekcja naturalna z przemiana fazowa (Natural convection with phase change) (in Polish). *IPPT PAN Report 8/97*, Warsaw.

Kowalewski, T., Cybulski, A. and Rebow, M. (1998) Particle image velocimetry and thermometry in freezing water, *Proc. 8th Flow Visualization Symp.*, Sorrento, Sept. 1998 (to appear).

Neumann, G. (1990) Three-dimensional numerical simulation of buoyancy-driven convection in vertical cylinders heated from below, *Journal of Fluid Mechanics*, **214**, 559–578.

Verzicco, R. and Camussi, R. (1997) Transitional regimes Prandtl thermal convection in a cylindrical cell, *Phy Fluids*, **9**, 1287–1295.

Wanschura, M., Kuhlmann, H.C. and Rath, H.J. (1996) dimensional instability of axisymmetric buoyant convec cylinders heated from below, *Journal of Fluid Mechanic* 399–415.